we assumed that a probe was subjected to founder hyper or hypomethylation, if $\Delta\beta > 0.3$ or $\Delta\beta < 0.3$ in all the samples of the case, respectively. Progressor methylations were identified as done for progressor CN alterations; we searched for differentially methylated probes among every pair of the sample groups divided by mutation-based evolutionary tree. For each probe, we obtained difference of mean methylation between every pair of the sample groups, and the maximum difference as a statistic $\Delta'\beta$. For a threshold value $\theta$, we obtained probes of which $|\Delta'\beta| > \theta$ as probes subjected to Progressor methylations. For each case, $\theta$ was adjusted so that FDR was 0.1. The FDR was calculated by permutation of the samples. The progressor methylations were further divided into progressor hyper and hypomethylations based on plus and minus of $\Delta\beta$ averaged across the samples. For making heat maps of multiregional methylation profiles in Fig 1, 10000 probes subjected to founder and progressor methylations were randomly sampled, due to the large number of the probes meeting the criteria. Similarly, Fig 4A was made for randomly sampled 6000 probes that had $|\Delta\beta| > 0.3$ at least one sample of any case, which seems sufficient to provide an overview of the methylomes.

## Analysis of methylation variance

For each probe, we calculated inter- and intra-variance (variance among cases and within cases). Our approach was based on partitioning of the sum of squares, which is utilized in ANOVA. Assuming that each of $k$ groups has $n_j$ variables, $x_{ij}$, the total sum of square $SS_T$ is decomposed into between- and within-group sum of squares, $SS_w$ and $SS_b$:

$$SS_T = SS_w + SS_b, \text{ where } ss_T = \sum_{j=1}^{k}\sum_{i=1}^{n_j}(x_{ij} - \bar{\bar{x}})^2,\ ss_w = \sum_{j=1}^{k}\sum_{i=1}^{n_j}(x_{ij} - \bar{x}_j)^2,\ ss_B = \sum_{j=1}^{k} n_j(\bar{x}_j - \bar{\bar{x}})^2,$$

$$\bar{x}_j = \sum_{i=1}^{n_j} x_{ij}/n_j, \text{ and } \bar{\bar{x}} = \sum_{j=1}^{k}\sum_{i=1}^{n_j} x_{ij} / \sum_{j=1}^{k} n_j.$$

In our setting, case 2–8 can be regarded as the k groups while the β-values of each sample can be regarded as $x_{ij}$. Inter- and intra-variance were measured by $SS_w$ and $SS_b$, respectively.

## Expression profiling

mRNA expression profiling were performed with oligonucleotide microarrays (Whole Human Genome Microarray Kit, 4x44K, Agilent Technologies) as described previously [34]. Multiregional gene expression profiles obtained from the microarray experiments were quantile normalized and subjected to the ComBat method [35] to remove batch effects. The EEM method [36] was then applied to the multiregional gene expression profile and the GO and curated Cp entries in MSigDB (http://www.broadinstitute.org/gsea/msigdb/), to obtain module activities of significant expression modules as expression signatures.

## Simulation

**1) The BEP model.** We computationally simulated BEP employing a cellular automaton model, which assumes each cell in a tumor as a cellular automaton (S16 Fig). A cell has a genome containing $n$ genes, each of which is represented as a binary value, 0 (wild) or 1 (mutated). Namely, the genome is represented as a binary vector $\boldsymbol{g}$ of length $n$. In a unit time step, each cell in the simulated tumor dies with a probability $q$. If the cell does not die, the cell then divides with a probability $p$. Before the cell division, we mutate the genome vector $g$: each of 0 elements of $g$ is set to 1 with a probability $r$. The first $d$ genes in $\boldsymbol{g}$ are assumed as driver genes, whose mutations accelerate the division speed. A normal cell without any mutations has a division probability $p_0$, and acquisition of one driver mutation increases $p$ by $10^f$-fold in the next time step; i.e., $p = p_0 \cdot 10^{fk}$, where $k = \sum^{d} g_i$, the number of mutated driver genes. The

death probability is fixed as $q = q_0$. Let $c$ and $t$ denote the size of the simulated cell population and the number of the time steps, respectively. We started a simulation with $c_0$ normal cells and repeated the unit time step while population size $c \leq c_{max}$ and time step $t \leq t_{max}$. A flowchart of the simulation was shown as S21A Fig. In this study, we set parameter values as follows: $n = 300$, $p_0 = 0.001$, $q_0 = 10^{-7}$, $c_0 = 10$, $c_{max} = 10^6$ and $t_{max} \simeq 5\times10^6$. $r$, $f$, and $d$ were subjected to parameter fitting as described below.

**2) Simulated tumor growth in a two-dimensional space.** We designed a simulated tumor to grow in a two-dimensional square lattice where each cell occupies one lattice point. In the beginning, $c_0$ cells are initialized as close as possible to the center of the lattice. When a cell dies, the occupied point is cleared and becomes empty. When a cell divides, we place the daughter cell in the neighborhood of the parent cell, assuming the Moore neighborhood (i.e., eight points surrounding a central point). If empty neighbor points exist, we randomly select one point from them. Otherwise, we create an empty point in any of the eight neighboring points by the following procedure. First, for each of the eight directions, we count the number of the consecutive occupied points that range from each neighboring points to immediately before the nearest empty cell as indicated in S21B Fig. Next, any of the eight directions is selected with a probability proportional with $1/l_i$, where $l_i$ ($1 \leq i \leq 8$) is the count of the consecutive occupied points for each direction. The consecutive occupied points in the selected direction are then shifted by one point so that an empty neighboring point appears as shown in S21C Fig. Note that simulation results are dependent on the order of the division operation in the two-dimensional square lattice. We first marked cells to be divided and applied the division operation to the marked cells along an outward spiral starting from the center. In each round on the spiral, the direction was randomly flipped in order to keep spatial symmetry. An example of such spirals was shown in S21D Fig.

**3) In silico multiregional sequencing.** We also performed multiregional sequencing of the simulated tumor in silico. We assumed 25 small square lattices of 31×31 that are evenly distributed in the whole square lattice where the tumor was spread (e.g. boxes in S21E Fig). To obtain multiregional profiles of $s$ samples, $s$ small square lattices were randomly selected from the small square lattices where at least a half of lattice points were occupied by cells (e.g. filled boxes in S21E Fig). In each of the $s$ regions, the proportions of mutated cells for each gene were obtained as a VAF. We then set VAFs that do not exceed 0.3 were set to 0; this filtering step was based on an assumption that multiregional sequencing misses low-frequency variants. Finally, the VAFs were represented as an $n\times s$ multiregional mutation profile matrix whose rows and columns represent genes and samples, respectively.

**4) Parameter fitting.** We fitted parameters of the BEP model to the real data by employing an approximate Bayesian computation approach [37]. Since the real multiregional mutation profiles were commonly characterized by the presence of founder and unique mutations, we focused on the proportion of founder and unique mutations per sample as summary statistics, $\varphi$ and $\theta$. Namely, for a given multiregional mutation profile matrix, $\varphi$ is obtained as the number of rows (genes) which have non-zero elements in all columns (samples), while $\theta$ is obtained by counting the number of rows which have non-zero elements uniquely in each column and averaging the number over the 5 columns.

We first obtained observed values of the summary statistics in the real multiregional mutation profiles of our 9 cases. Since $\varphi$ and $\theta$ are dependent on the number of multiregional samples, we fixed $s$ to 5, which is the minimum number of samples in the 9 cases. For case 4 and 9, which contained 5 samples in each, we simply calculated $\varphi$ and $\theta$. For the other samples that contained more than 5 samples, we performed downsampling to obtain 10 mutation profile matrices of 5 samples, and averaged $\varphi$ and $\theta$ over the 10 trials. S17A Fig shows $\varphi$ and $\theta$ while S17B Fig shows multiregional mutation profiles for each case. From $\varphi$ and $\theta$ of the 9 cases, we

estimated the observed values as $\varphi = 0.718 \pm 0.115$ and $\theta = 0.138 \pm 0.040$ (mean±standard deviation).

We next performed the simulation with different parameter settings to evaluate which parameter setting leads to summary statistic values similar to the observed ones. Here, d (the number of driver genes), f (strength of driver genes) and r (mutation rate) were subjected to parameter fitting analysis. We prepared 10 integers from 1 to 10 as *d*; 10 numbers from 0.1 to 1.0 incremented by 0.1 as *f*; and 0.0001, 0.0003, 0.001, 0.003, and 0.01 as *r*, and take every combination of the parameter values as done in grid search. This leads to $10 \times 10 \times 5 = 500$ parameter settings, for each of which the BEP simulation was repeated 50 times. For the 50 simulated tumors from each parameter setting, we then performed in silico multiregional sequencing with $s = 5$ to obtain $\varphi$ and $\theta$. Finally, for each parameter setting, the proportion of instances whose statistics (both $\varphi$ and $\theta$) fall within 1 standard deviation from the mean of the observed values was calculated and visualized as heat maps in S18A Fig. From this data, we found that the BEP model can produce multiregional profiles similar to those of our 9 cases if a high mutation rate, a sufficient number and sufficient strength of driver genes (e.g., $r = 0.01$, $d \geqq 0.4$ and $f \geqq 0.8$) are assumed. S18B Fig shows representative multiregional mutation profile matrices from simulations with such parameter settings.

**5) Analysis and visualization of simulation data.** Based on the parameter fitting analysis, we fixed parameter as $r = 0.01$, $d = 6$, and $f = 0.8$ in the following analysis. From a tumor simulated with this parameter setting, we randomly sampled *m* cells (here, we set $m = 500$) to obtain an $n \times m$ single-cell mutation profile matrix, each of whose *m* columns is the *n*-dimensional genome vector $\boldsymbol{g}$ for each cell. We obtained color labels for each cell, as done for the sample color labels in the real data. Namely, we applied principal component analysis to the single-cell mutation profile matrix and mixed RGB colors according to dimension-reduced genome vectors. Each cell on the two-dimensional square lattice was colored with the corresponding color label (Fig 5A). The single-cell mutation profile matrix was visualized as a cluster heat map together with the color labels on the top (Fig 5B). We also applied in silico multiregional profiling with $s = 8$ to obtain a multiregional mutation profile matrix, which was also visualized as a heat map (Fig 5C). Its color labels were prepared using the PCA loading vectors calculated from the single-cell mutation profile matrix. Evolutionary snapshots of the same tumor were presented in S20 Fig while four other instances from independent simulation trials were presented in S19 Fig. To calculate the distribution of VAFs (Fig 5D) and proportion of driver genes (Fig 5E) in different categories of mutations, 20 multiregional mutation profile matrices were obtained from independent simulation trials. Rows of the 10 matrices were then categorized into "founder" (having non-zero elements in all columns), "shared" (having non-zero elements in not all but multiple columns), "unique" (having non-zero elements uniquely in any column), and "unmutated" (having zero elements in all columns). The distribution of VAFs was obtained by extracting non-zero elements from the rows of each category. The proportion of driver genes was obtained by counting rows associated with driver genes in the rows of each category.

## Supporting Information

**S1 Fig. Depth of whole exome sequencing.** (A) Mean depth of each sample. (B) Fractions of the target region covered with at least 10x, 20x and 30x depth.
(PDF)

**S2 Fig. Evidence of subclonal mixing.** We searched for progressor mutations that were shared by distant branches in the evolutionary trees of the 9 cases, and found clear examples of such singular mutations in case3 and case7. The heat maps show VAFs of the singular mutations

from exome and targeted deep sequencing for case3 and case7, respectively. Timings of subclonal mixing events were inferred and indicated by red arrows on the evolutional trees.
(PDF)

**S3 Fig. Pathway-level view of genomic ITH.** (A) The color table shows whether any member of the 5 driver pathways was disrupted by founder and progressor genomic alterations (i.e., mutations or focal CN alterations) in the 9 cases. The driver pathways and their members were obtained from the TCGA paper [8]. (B) Genomic alteration profiles of the driver pathway members in each of the 9 cases.
(PDF)

**S4 Fig. The number of founder, shared and unique mutations.**
(PDF)

**S5 Fig. Correlations between mutation counts and patients' ages.** In addition to our data, multiregional mutation data from previous clear cell renal cell carcinoma [3] and pancreatic cancer [2] studies were analyzed. ρ's are Spearman's correlation coefficients.
(PDF)

**S6 Fig. Validation for using clonal and subclonal mutations as surrogates of founder and progressor mutations.** (**A**) The Sciclone analysis [38] was performed on three representative samples. (**B**) For each of the clonal and subclonal mutations estimated based on cancer cell fraction, proportions of founder, shared and unique mutations were presented. This analysis was performed for samples whose purities exceed 0.6. The result demonstrated that, when we focused on each single sample, founder and progressor mutations tended to exist as clonal and subclonal mutations, respectively.
(PDF)

**S7 Fig. Mutational analysis using TCGA data.** (**A**) Correlations between mutation rates and patients' ages. P-values were calculated by The Wilcoxon rank-sum test. (**B**) Mutational signature analysis. (**C**) For each base substitution type, the number of patients having the larger number of clonal or subclonal mutations was shown. P-values were calculated by the binomial test.
(PDF)

**S8 Fig. Mutational signatures in the trinucleotide context.** (A) Founder and progresor mutations in the 9 cases were divided into 96 substitution patterns based on mutated bases and their 5' and 3' flanking bases, and the percentages of each substitution pattern were plotted as a bar plot. (B) Clonal and subclonal mutations in the TCGA samples were analyzed as in A.
(PDF)

**S9 Fig. Multiregional CN profiles.** The heat maps show LRR across chromosomes in each sample.
(PDF)

**S10 Fig. Density plot showing distributions of inter- and intratumor variance for each category of probes.**
(PDF)

**S11 Fig. Classification of the CIMP and non-CIMP subtypes.** Methylation datasets of 529 TCGA COADREAD samples were obtained from https://tcga-data.nci.nih.gov/tcga/. For the 2000 probes showing the highest variance in the TCGA samples, we made clustered heat maps of β values for only the TCGA samples (**A**) and the TCGA samples mixed with our samples

(**B**). Based on this result, we classified cases 5 and 9 into the CIMP subtype.
(PDF)

**S12 Fig. Differential contribution of different types of epigenetic domains to intratumor and intertumor variance.** Enrichment scores for intratumor (A) and intertumor (B) variance were calculated as in Fig 4B. Classification of chromosomal regions was based epigenetic status in normal colon tissue, which is profiled by the NIH Roadmap Epigenomics Consortium [13].
(PDF)

**S13 Fig. The number of probes subjected to founder and progressor methylation.**
(PDF)

**S14 Fig. Multiregional methylation profiles of epigenetic marker genes.** The heat map shows $\Delta\beta$ values of probes contained by the CpG island promoters of the epigenetic gatekeepers [14] and CIMP-related genes [39].
(PDF)

**S15 Fig. Correlations between methylation and patients' ages in the TGGA samples.** We assumed that hyper- and hypomethylated probes have $\Delta\beta > 0.3$ and $\Delta\beta < -0.3$, respectively. CpG island hypermethylation was significantly correlated with patients' ages. r's are Pearson's correlation coefficients and p-values were calculated by the Pearson's correlation test.
(PDF)

**S16 Fig. A schema of the BEP model.** A cell has n genes, d out of which are driver genes. In this schema, n = 10 and d = 4, and red and blue boxes denote driver and non-drive genes, respectively. In a unit time step, a cell divides or dies with probabilities p and q, respectively. During each cell division, each gene is randomly mutated with a probability r, and one driver mutation, which is denoted by a red cross, increases p by $10^f$-fold.
(PDF)

**S17 Fig. Parameter fitting 1.** (**A**) Observed values of summary statistics in the real data. The proportion of founder and unique mutations were obtained for 9 cases. For each of the cases except case4 and case9, downsamplings were performed to obtain 10 multiregional profiles of 5 samples and the statistics were averaged over the downsampling trials. The error bars indicate standard deviations for the downsampling trials. Finally, an "average" over the 9 cases was obtained as an estimate of the observed value of each summary statistic. The error bars at "average" indicate standard deviations over the 9 cases. (**B**) Multiregional mutation profiles from the real experiments. For the cases except case4 and case9, representative samples from the 10 downsampling trials were presented as in Fig 5C.
(PDF)

**S18 Fig. Parameter fitting 2.** (**A**) The proportion of simulation instances fitted to the real data. The proportion of simulation instances whose statistics fall within 1 standard deviation from the mean of the observed values was calculated for each parameter settings and visualized as heat maps (**B**) Multiregional mutation profiles from the simulations. Representative instances from simulation with indicated parameter settings were presented as in Fig 5C. Left blue bars indicate driver genes.
(PDF)

**S19 Fig. Four tumors from independent simulation trials.** Simulated tumors, simulated single-cell and multiregional mutation profile matrix from four simulation trials are shown as in Fig 5A–5C.
(PDF)

**S20 Fig. Simulated tumor growth.** (**A**) Snap shots of growing tumors in a simulation. Differently colored cell populations represent each clone. (**B**) A growth curve of the simulated tumor. The snap shots were obtained at each plotted point. (**C**) Single-cell mutation profiles of the simulated tumor during growth. Timing at which the mutation profiles were obtained are indicated by red rectangles in (**A**) and red plotted points in (**B**). Top colored bars represent each clone while left blue bars represent driver genes.
(PDF)

**S21 Fig. Illustration of our simulation method.** (**A**) A flowchart of our simulation. (**B, C, D,** and **E,**) illustration of division operation. See the simulation section in Materials and Methods.
(PDF)

**S1 Table. Information of 9 colorectal cancer cases.**
(XLSX)

**S2 Table. Information of 84 analyzed samples.**
(XLSX)

**S3 Table. Information of detected mutations.**
(XLSX)

## Acknowledgments

We thank to Ms. Shimo-oka, Ms. Kasagi, Ms. Kohno, Ms. Oda, Ms. Kawano and Ms. Aoyagi for their assistance. We gratefully acknowledge the TCGA Consortium and all its members for TCGA Project. This research used computational resources of the K computer provided by the RIKEN Advanced Institute for Computational Science through the HPCI System Research project (Project ID: hp140230). Computation time was also provided by the Super Computer System, Human Genome Center, Institute of Medical Science, University of Tokyo.

## Author Contributions

Conceived and designed the experiments: YT AN KM MM SM TS MK SY KYamad SN SS HIi. Performed the experiments: YT RU GS YSu KYo HA GN KYamam YN TIw JK. Analyzed the data: RU AN HHi TS GS HHa. Contributed reagents/materials/analysis tools: AN KC YShin KSu HE TIg YShir MM SK YD HY YM EO YO KSh HS SO HIs. Wrote the paper: YT RU AN SO.

## References

1. McGranahan N, Swanton C. Biological and Therapeutic Impact of Intratumor Heterogeneity in Cancer Evolution. Cancer cell. 2015; 27(1):15–26. Epub 2015/01/15. doi: 10.1016/j.ccell.2014.12.001 PMID: 25584892.
2. Yachida S, Jones S, Bozic I, Antal T, Leary R, Fu B, et al. Distant metastasis occurs late during the genetic evolution of pancreatic cancer. Nature. 2010; 467(7319):1114–7. doi: 10.1038/nature09515 PMID: 20981102; PubMed Central PMCID: PMC3148940.
3. Gerlinger M, Horswell S, Larkin J, Rowan AJ, Salm MP, Varela I, et al. Genomic architecture and evolution of clear cell renal cell carcinomas defined by multiregion sequencing. Nature genetics. 2014; 46 (3):225–33. doi: 10.1038/ng.2891 PMID: 24487277.
4. de Bruin EC, McGranahan N, Mitter R, Salm M, Wedge DC, Yates L, et al. Spatial and temporal diversity in genomic instability processes defines lung cancer evolution. Science. 2014; 346(6206):251–6. doi: 10.1126/science.1253462 PMID: 25301630.
5. Zhang J, Fujimoto J, Zhang J, Wedge DC, Song X, Zhang J, et al. Intratumor heterogeneity in localized lung adenocarcinomas delineated by multiregion sequencing. Science. 2014; 346(6206):256–9. doi: 10.1126/science.1256930 PMID: 25301631.

6. Aryee MJ, Liu W, Engelmann JC, Nuhn P, Gurel M, Haffner MC, et al. DNA methylation alterations exhibit intraindividual stability and interindividual heterogeneity in prostate cancer metastases. Science translational medicine. 2013; 5(169):169ra10. Epub 2013/01/25. doi: 10.1126/scitranslmed.3005211 PMID: 23345608; PubMed Central PMCID: PMCPMC3577373.

7. Brocks D, Assenov Y, Minner S, Bogatyrova O, Simon R, Koop C, et al. Intratumor DNA methylation heterogeneity reflects clonal evolution in aggressive prostate cancer. Cell reports. 2014; 8(3):798–806. doi: 10.1016/j.celrep.2014.06.053 PMID: 25066126.

8. Cancer Genome Atlas N. Comprehensive molecular characterization of human colon and rectal cancer. Nature. 2012; 487(7407):330–7. doi: 10.1038/nature11252 PMID: 22810696; PubMed Central PMCID: PMC3401966.

9. Hall BG. Building phylogenetic trees from molecular data with MEGA. Molecular biology and evolution. 2013; 30(5):1229–35. Epub 2013/03/15. doi: 10.1093/molbev/mst012 PMID: 23486614.

10. Sottoriva A, Kang H, Ma Z, Graham TA, Salomon MP, Zhao J, et al. A Big Bang model of human colorectal tumor growth. Nature genetics. 2015; 47(3):209–16. Epub 2015/02/11. doi: 10.1038/ng.3214 PMID: 25665006.

11. Alexandrov LB, Nik-Zainal S, Wedge DC, Aparicio SA, Behjati S, Biankin AV, et al. Signatures of mutational processes in human cancer. Nature. 2013; 500(7463):415–21. doi: 10.1038/nature12477 PMID: 23945592; PubMed Central PMCID: PMC3776390.

12. Hinoue T, Weisenberger DJ, Lange CP, Shen H, Byun HM, Van Den Berg D, et al. Genome-scale analysis of aberrant DNA methylation in colorectal cancer. Genome research. 2012; 22(2):271–82. Epub 2011/06/11. doi: 10.1101/gr.117523.110 PMID: 21659424; PubMed Central PMCID: PMCPMC3266034.

13. Kundaje A, Meuleman W, Ernst J, Bilenky M, Yen A, Heravi-Moussavi A, et al. Integrative analysis of 111 reference human epigenomes. Nature. 2015; 518(7539):317–30. Epub 2015/02/20. doi: 10.1038/nature14248 PMID: 25693563; PubMed Central PMCID: PMCPMC4530010.

14. Jones PA, Baylin SB. The epigenomics of cancer. Cell. 2007; 128(4):683–92. doi: 10.1016/j.cell.2007.01.029 PMID: 17320506; PubMed Central PMCID: PMC3894624.

15. Ahuja N, Li Q, Mohan AL, Baylin SB, Issa JP. Aging and DNA methylation in colorectal mucosa and cancer. Cancer research. 1998; 58(23):5489–94. Epub 1998/12/16. PMID: 9850084.

16. Niida A, Ito S, Tremmel G, Imoto S, Uchi R, Takahashi Y, et al. Cancer evolution simulation identifies possible principles underlying intratumor heterogeneity; 2015. Preprint. Available: bioRxiv. doi: 10.1101/022806 Accessed 1 September 2015.

17. Lopez-Otin C, Blasco MA, Partridge L, Serrano M, Kroemer G. The hallmarks of aging. Cell. 2013; 153(6):1194–217. Epub 2013/06/12. doi: 10.1016/j.cell.2013.05.039 PMID: 23746838; PubMed Central PMCID: PMCPMC3836174.

18. Welch JS, Ley TJ, Link DC, Miller CA, Larson DE, Koboldt DC, et al. The origin and evolution of mutations in acute myeloid leukemia. Cell. 2012; 150(2):264–78. Epub 2012/07/24. doi: 10.1016/j.cell.2012.06.023 PMID: 22817890; PubMed Central PMCID: PMCPMC3407563.

19. Jacobs KB, Yeager M, Zhou W, Wacholder S, Wang Z, Rodriguez-Santiago B, et al. Detectable clonal mosaicism and its relationship to aging and cancer. Nature genetics. 2012; 44(6):651–8. doi: 10.1038/ng.2270 PMID: 22561519; PubMed Central PMCID: PMC3372921.

20. Xie M, Lu C, Wang J, McLellan MD, Johnson KJ, Wendl MC, et al. Age-related mutations associated with clonal hematopoietic expansion and malignancies. Nature medicine. 2014; 20(12):1472–8. doi: 10.1038/nm.3733 PMID: 25326804; PubMed Central PMCID: PMC4313872.

21. Tomasetti C, Vogelstein B. Cancer etiology. Variation in cancer risk among tissues can be explained by the number of stem cell divisions. Science. 2015; 347(6217):78–81. Epub 2015/01/03. doi: 10.1126/science.1260825 PMID: 25554788.

22. Wang Y, Waters J, Leung ML, Unruh A, Roh W, Shi X, et al. Clonal evolution in breast cancer revealed by single nucleus genome sequencing. Nature. 2014; 512(7513):155–60. doi: 10.1038/nature13600 PMID: 25079324; PubMed Central PMCID: PMC4158312.

23. Diaz LA Jr., Williams RT, Wu J, Kinde I, Hecht JR, Berlin J, et al. The molecular evolution of acquired resistance to targeted EGFR blockade in colorectal cancers. Nature. 2012; 486(7404):537–40. Epub 2012/06/23. doi: 10.1038/nature11219 PMID: 22722843; PubMed Central PMCID: PMCPMC3436069.

24. Muto T, Bussey HJ, Morson BC. The evolution of cancer of the colon and rectum. Cancer. 1975; 36(6):2251–70. Epub 1975/12/01. PMID: 1203876.

25. Fearon ER, Vogelstein B. A genetic model for colorectal tumorigenesis. Cell. 1990; 61(5):759–67. Epub 1990/06/01. PMID: 2188735.

26. Jones S, Chen WD, Parmigiani G, Diehl F, Beerenwinkel N, Antal T, et al. Comparative lesion sequencing provides insights into tumor evolution. Proceedings of the National Academy of Sciences of the

United States of America. 2008; 105(11):4283–8. Epub 2008/03/14. doi: 10.1073/pnas.0712345105 PMID: 18337506; PubMed Central PMCID: PMCPMC2393770.

27. Markowitz SD, Bertagnolli MM. Molecular origins of cancer: Molecular basis of colorectal cancer. The New England journal of medicine. 2009; 361(25):2449–60. Epub 2009/12/19. doi: 10.1056/NEJMra0804588 PMID: 20018966; PubMed Central PMCID: PMCPMC2843693.

28. Zeuner A, Todaro M, Stassi G, De Maria R. Colorectal cancer stem cells: from the crypt to the clinic. Cell stem cell. 2014; 15(6):692–705. Epub 2014/12/07. doi: 10.1016/j.stem.2014.11.012 PMID: 25479747.

29. Sottoriva A, Graham T. A pan-cancer signature of neutral tumor evolution; 2015. Preprint. Available: *bioRxiv*. *doi:* 10.1101/014894 *Accessed* 1 *September* 2015.

30. Takatsuno Y, Mimori K, Yamamoto K, Sato T, Niida A, Inoue H, et al. The rs6983267 SNP is associated with MYC transcription efficiency, which promotes progression and worsens prognosis of colorectal cancer. Annals of surgical oncology. 2013; 20(4):1395–402. Epub 2012/09/15. doi: 10.1245/s10434-012-2657-z PMID: 22976378.

31. Shiraishi Y, Sato Y, Chiba K, Okuno Y, Nagata Y, Yoshida K, et al. An empirical Bayesian framework for somatic mutation detection from cancer genome sequencing data. Nucleic acids research. 2013; 41 (7):e89. Epub 2013/03/09. doi: 10.1093/nar/gkt126 PMID: 23471004; PubMed Central PMCID: PMCPMC3627598.

32. Van Loo P, Nordgard SH, Lingjaerde OC, Russnes HG, Rye IH, Sun W, et al. Allele-specific copy number analysis of tumors. Proceedings of the National Academy of Sciences of the United States of America. 2010; 107(39):16910–5. Epub 2010/09/15. doi: 10.1073/pnas.1009843107 PMID: 20837533; PubMed Central PMCID: PMCPMC2947907.

33. Lohr JG, Stojanov P, Carter SL, Cruz-Gordillo P, Lawrence MS, Auclair D, et al. Widespread genetic heterogeneity in multiple myeloma: implications for targeted therapy. Cancer cell. 2014; 25(1):91–101. Epub 2014/01/18. doi: 10.1016/j.ccr.2013.12.015 PMID: 24434212; PubMed Central PMCID: PMCPMC4241387.

34. Takahashi Y, Sheridan P, Niida A, Sawada G, Uchi R, Mizuno H, et al. The AURKA/TPX2 axis drives colon tumorigenesis cooperatively with MYC. Annals of oncology: official journal of the European Society for Medical Oncology / ESMO. 2015. Epub 2015/01/30. doi: 10.1093/annonc/mdv034 PMID: 25632068.

35. Johnson WE, Li C, Rabinovic A. Adjusting batch effects in microarray expression data using empirical Bayes methods. Biostatistics (Oxford, England). 2007; 8(1):118–27. Epub 2006/04/25. doi: 10.1093/biostatistics/kxj037 PMID: 16632515.

36. Niida A, Smith AD, Imoto S, Aburatani H, Zhang MQ, Akiyama T. Gene set-based module discovery in the breast cancer transcriptome. BMC bioinformatics. 2009; 10:71. doi: 10.1186/1471-2105-10-71 PMID: 19243633; PubMed Central PMCID: PMC2674431.

37. Csillery K, Blum MG, Gaggiotti OE, Francois O. Approximate Bayesian Computation (ABC) in practice. Trends in ecology & evolution. 2010; 25(7):410–8. Epub 2010/05/22. doi: 10.1016/j.tree.2010.04.001 PMID: 20488578.

38. Miller CA, White BS, Dees ND, Griffith M, Welch JS, Griffith OL, et al. SciClone: inferring clonal architecture and tracking the spatial and temporal patterns of tumor evolution. PLoS computational biology. 2014; 10(8):e1003665. doi: 10.1371/journal.pcbi.1003665 PMID: 25102416; PubMed Central PMCID: PMC4125065.

39. Weisenberger DJ, Siegmund KD, Campan M, Young J, Long TI, Faasse MA, et al. CpG island methylator phenotype underlies sporadic microsatellite instability and is tightly associated with BRAF mutation in colorectal cancer. Nature genetics. 2006; 38(7):787–93. Epub 2006/06/29. doi: 10.1038/ng1834 PMID: 16804544.

Hepatology Research

*Hepatology Research* 2016 doi: 10.1111/hepr.12674

*Original Article*

# Sarcopenia is a poor prognostic factor following hepatic resection in patients aged 70 years and older with hepatocellular carcinoma

Norifumi Harimoto, Tomoharu Yoshizumi, Masahiro Shimokawa, Kazuhito Sakata, Kouichi Kimura, Shinji Itoh, Toru Ikegami, Tetsuo Ikeda, Ken Shirabe and Yoshihiko Maehara

*Department of Surgery and Science, Graduate School of Medical Sciences, Kyushu University, Fukuoka, Japan*

*Aim:* The present study investigated the effect of sarcopenia on short- and long-term surgical outcomes and identified potential prognostic factors for hepatocellular carcinoma (HCC) following hepatectomy among patients 70 years of age and older.

*Methods:* Patient data were retrospectively collected for 296 consecutive patients who underwent hepatectomy for HCC with curative intent. Patients were assigned to two groups according to age (younger than 70 years, and 70 years and older), and the presence of sarcopenia. The clinicopathological, surgical outcome, and long-term survival data were analyzed.

*Results:* Sarcopenia was present in 112 of 296 (37.8%) patients with HCC, and 35% of patients aged 70 years and older. Elderly patients had significantly lower serum albumin levels, prognostic nutrition index, percentage of liver cirrhosis, and histological intrahepatic metastasis compared with patients younger than 70 years. Overall survival and disease-free survival rates in patients with sarcopenia correlated with significantly poor prognosis in the group aged 70 years and older. Multivariate analysis revealed that sarcopenia was predictive of an unfavorable prognosis.

*Conclusion:* This retrospective analysis revealed that sarcopenia was predictive of worse overall survival and recurrence-free survival after hepatectomy in patients 70 years of age and older with HCC.

**Key words:** elderly, hepatectomy, hepatocellular carcinoma, prognosis, sarcopenia

## INTRODUCTION

THE WORLD'S POPULATION is rapidly ageing. Between 2000 and 2050, the proportion of the world's population aged over 60 years will double from approximately 11% to 22%[1] and the age of patients with some malignancies has also been increasing. In such a society, abuse of elderly people is an important public health problem. In 1989, Irwin Rosenberg[2] proposed the term "sarcopenia" to describe the age-related decline of muscle mass. Sarcopenia is a syndrome characterized by the progressive and generalized loss of skeletal muscle mass and strength, with a risk of adverse outcomes such as physical disability, poor quality of life, and death.[3–5] It is the result of multiple physiologic derangements, ultimately resulting in an insidious functional decline. Skeletal muscle mass is highly important in immune function, glucose disposal, protein synthesis, and mobility; therefore, decreases in skeletal muscle can result in a plethora of physiologic impairments.[6] Traditional measures of nutritional assessment, such as body mass index and serum albumin, do not accurately predict outcome in the injured elderly. In the future aging society, patients with sarcopenia will be a social issue.

Sarcopenia represents not only a potential new predictor for mortality and discharge disposition, but was also identified as a poor prognostic factor for pancreatic cancer, colorectal liver metastases, melanoma, liver cirrhosis, and liver transplantation.[7–12] We previously published that sarcopenia was predictive of a worse OS even when adjusted for other known predictors in 186 patients with HCC after hepatectomy.[13] Because of advances in the diagnosis and management of HCC, significant improvements in OS and DFS rates for HCC after hepatectomy have been

*Correspondence: Dr Tomoharu Yoshizumi, Department of Surgery and Science, Graduate School of Medical Sciences, Kyushu University, 3-1-1 Maidashi, Higashi-ku, Fukuoka 812-8582, Japan. Email: yosizumi@surg2.med.kyushu-u.ac.jp*

*Conflict of interest:* The authors have no conflict of interest.

*Received 10 September 2015; revision 22 October 2015; accepted 10 February 2016.*

achieved. In particular, sufficient evidence exists that hepatectomy can be safely undertaken in selected elderly patients.[14–16] However, even when curative resection is carried out, a considerable number of patients develop intrahepatic or extrahepatic recurrence postoperatively. The prognostic assessment of patients with HCC after hepatectomy and recurrence in this population are important clinical issues.[17–19] Both tumor- and host-related factors are related to the clinical outcome, but it is difficult to evaluate the general condition of patients excluding liver function before hepatectomy, especially in elderly patients. Conventional methods, such as the Child–Pugh classification, were the first systematic approaches used to determine the severity of cirrhosis and select the patients who could tolerate hepatic resection; however, these methods do not reflect the patient's general condition. Given this background, predicting the clinical and prognostic outcome of HCC patients in elderly is of considerable importance.

In this study, a retrospective study was carried out at our institution to investigate the outcome of elderly patients with sarcopenia who underwent hepatic resection. The outcome of these patients was compared to that of patients without sarcopenia undergoing hepatic resection during the same period.

## METHODS

### Patient characteristics

ALL PATIENTS WHO underwent curative hepatic resection as initial treatment at the Department of Surgery II, Kyushu University Hospital (Fukuoka, Japan) from January 2004 to December 2013 were enrolled in this study. Curative resection was defined as complete macroscopic removal of the tumor. All patients underwent preoperative CT in Kyushu University Hospital. A transverse CT image of the third lumbar vertebrae (L3) in the inferior direction was assessed from each scan. Skeletal muscle was identified and quantified by Hounsfield unit thresholds of −29 to +150 according to a previous report.[8,13] According to the Hounsfield unit scale, the radiodensity of water is 0 U and that of air is −1000 U. Multiple muscles were identified, including the psoas, erector spinae, quadratus lumborum, transversus abdominis, external and internal obliques, and rectus abdominis as a previous report. The CT measurement was calibrated with water and air at fixed intervals. The cross-sectional areas ($cm^2$) of skeletal muscles in the L3 region were measured by manual outlining on the CT images and checked by the radiologist. The formulae to calculate skeletal muscle area were $126.9 \times BSA - 66.2$ in men and $125.6 \times BSA - 81.1$ in women according to a previous report by Yoshizumi *et al.*[20] Using these formulae, sarcopenia in Japanese patients was defined so that the actual skeletal muscle area was 85% smaller than the calculated skeletal muscle area. The clinicopathological backgrounds and rates of OS and RFS were compared between the two groups, which were divided according to the presence of sarcopenia.

The prognostic factors were examined with respect to OS and RFS on the basis of the following variables: sarcopenia (absence vs presence); skeletal muscle mass; age; gender (male vs female); body mass index; HBs Ag (HBs Ag[+] vs HBs Ag[−]); HCV antibody (HCV[+] vs HCV[−]; serum albumin level; serum total bilirubin level; serum aspartate aminotransferase level; platelet number; ICGR15; C reactive protein; PNI; Child–Pugh classification (A vs B); histological liver cirrhosis (normal liver + chronic hepatitis vs liver fibrosis and liver cirrhosis); tumor size; tumor number (solitary vs multiple); TNM stage according to the Liver Cancer Study Group in Japan[21] (I + II vs III + IV); tumor differentiation (well differentiated + moderately differentiated vs poorly differentiated); microvascular invasion (absence vs presence); im (absence vs presence); serum α-fetoprotein level; des-γ-carboxy prothrombin level; operative procedure (anatomical vs non-anatomical); operative time; estimated blood loss; and postoperative complication (absence vs presence). The patients with diabetes were defined as the use of oral hypoglycemic agent or insulin. Postoperative complications within 1 month after hepatectomy, included liver failure, encephalopathy, gastrointestinal bleeding, i.p. abscess, abdominal hemorrhage, bile leakage, pleural effusion, intractable ascites, and wound infection. The more severe Clavien–Dindo grade III complications,[22] which required surgical interventions, were defined as the presence of postoperative complication.

### Surgical procedures

The details of surgical techniques and patient selection criteria have been reported previously.[19] Our criteria for hepatic resection were that ascites was not detected or were controllable by diuretics, serum total bilirubin level was <2.0 mg/mL, and the ICGR15 value was less than 40%. These included a J-shaped incision for routine abdominal access, a slow and gentle hepatic dissection using an ultrasonic dissector with a coagulator (CUSA Excel; Integra, Plainsboro, NJ, USA), with systematic ligation of all sizable vessels, and close ultrasonographic guidance along the transection line. Cholecystectomy was carried out in all patients if the gallbladder was present. An intraoperative bile leakage test was routinely undertaken to identify bile leakage. With this procedure, we recognized small bile leakage sites on the cut liver surface and could repair them by Z-suturing using 6-0PDSII (Johnson & Johnson, Tokyo,

Japan). Intraoperative vascular control was achieved by the Pringle maneuver.[24]

## Follow-up strategy and recurrence pattern

After discharge, all patients were examined for recurrence by ultrasonography and tumor markers, such as α-fetoprotein and des-γ-carboxy prothrombin, every month and by CT every 6 months. When recurrence was suspected, additional examination such as hepatic angiography were carried out. We treated recurrent HCC by repeat hepatectomy, ablation therapy, and lipiodolization, according to a strategy described previously.[25]

## Histological study

All of the resected specimens were cut into serial 5–10-mm-thick slices and fixed in 10% formalin. After

**Table 1** Comparison of clinicopathological factors between two groups of patients with hepatocellular carcinoma (HCC), classified by age

| Variables | <70 years ($n$ = 157) | ≥70 years ($n$ = 139) | $P$-value |
|---|---|---|---|
| Male / female | 123/34 | 98/41 | 0.122 |
| HBV | 20 (18.0%) | 8 (10.1%) | 0.243 |
| HCV | 65 (58.6%) | 51 (68.0%) | 0.250 |
| Skeletal muscle mass, $cm^2/m^2$ | 74.4 ± 11.9 | 70.9 ± 12.8 | 0.018 |
| Sarcopenia (+) | 55 (35.0%) | 57 (41.0%) | 0.337 |
| Body mass index, $kg/m^2$ | 22.8 ± 3.1 | 23.1 ± 3.3 | 0.356 |
| Diabetes mellitus | 49 (31.2%) | 38 (27.3%) | 0.495 |
| Albumin, g/dL | 4.0 ± 0.5 | 3.9 ± 0.5 | 0.009 |
| Total bilirubin, mg/dL | 0.8 ± 0.4 | 0.7 ± 0.4 | 0.307 |
| AST, IU/L | 51 ± 36 | 56 ± 46 | 0.475 |
| Platelet count, $10^4/\mu L$ | 15.4 ± 6.4 | 16.3 ± 6.8 | 0.230 |
| ICGR15, % | 13.8 ± 7.6 | 14.7 ± 7.4 | 0.337 |
| CRP | 0.41 ± 1.2 | 0.41 ± 1.8 | 0.997 |
| PNI | **48.4 ± 6.3** | **46.1 ± 6.4** | 0.002 |
| Child–Pugh A / B | 151/6 | 131/8 | 0.190 |
| Hepatitis grade, none / mild / severe | 13/80/18 | 11/55/9 | 0.652 |
| Liver cirrhosis, nl + ch/lf + lc | 71/86 | 83/56 | 0.006 |
| Tumor size, cm | 4.0 ± 3.2 | 4.0 ± 2.9 | 0.989 |
| Solitary / multiple | 121/36 | 113/23 | 0.171 |
| Stage, I / II / III / IV | 24/83/39/11 | 24/73/35/7 | 0.884 |
| Differentiation, well / mod / poor | 10/77/24 | 9/50/16 | 0.690 |
| mvi (+) | 53 (33.7%) | 48 (34.5%) | 0.889 |
| im (+) | 30 (19.1%) | 12 (8.6%) | 0.010 |
| AFP, ng/mL | 5569 ± 47 209 | 74 838 ± 15 567 | 0.529 |
| DCP, mAU/L | 3831 ± 14 797 | 3685 ± 22 463 | 0.947 |
| Anatomical / non-anatomical | 76/35 | 47/28 | 0.508 |
| Operative time, min | 368 ± 114 | 355 ± 154 | 0.512 |
| Estimated blood loss, g | 648 ± 528 | 885 ± 2887 | 0.398 |
| Blood transfusion (+) | 12(10.8%) | 10(13.3%) | 0.649 |
| Postoperative complications | 29 (18.4%) | 22 (15.8%) | 0.613 |
| Postoperative hospital stay, days | 18 ± 18 | 17 ± 15 | 0.501 |

Data are expressed as means ± standard deviations or number of patients (percentage) as appropriate. AFP, α-fetoprotein; AST, aspartate aminotransferase; ch, chronic hepatitis; CRP, C reactive protein; DCP, des-γ-carboxy prothrombin; HBV, hepatitis B antigen-positive; HCV, hepatitis C antibody-positive; ICGR15, indocyanine green dye retention test at 15 min; im, intrahepatic metastasis; lc, liver cirrhosis; lf, liver fibrosis; mod, moderately differentiated HCC; mvi, microvascular invasion; nl, normal liver; poor, poorly differentiated HCC; PNI, prognostic nutrition index; Stage, TNM stage defined by the Liver Cancer Study Group of Japan; well, well differentiated HCC.

macroscopic examination, the slice with the greatest dimensions was trimmed for embedding in paraffin and cut into 4-μm microscopic sections. The sections were stained with hematoxylin–eosin. Tumor differentiation, microvascular invasion, im, and histological liver cirrhosis were examined by the pathologist according to the guidelines of the Liver Cancer Study Group in Japan.

### Statistical analysis

The associations of continuous and categorical variables with the relevant outcome variables were assessed using Student's *t*-test and the $\chi^2$-test, respectively. The survival curves and RFS after hepatectomy of the two groups were analyzed by the Kaplan–Meier method and compared with the log-rank test. To identify the prognostic factors after hepatectomy, all variables over $P < 0.1$ in univariate analysis were included in the multivariate Cox proportional model in the analyses of both OS and RFS.

All analyses were carried out with Statview 5.0 software (Abacus Concepts Inc., Berkeley, CA, USA). *P*-values less than 0.05 were considered statistically significant.

## RESULTS

IN TOTAL, SARCOPENIA was identified in 112 patients (37.8%): 83 men and 29 women among the 296 patients with HCC. Sarcopenia was identified in 35% of patients aged 70 years or older. The clinicopathological characteristics of all patients are shown in Table 1. Skeletal muscle in patients aged 70 years and older was significantly smaller than in patients younger than 70 years,

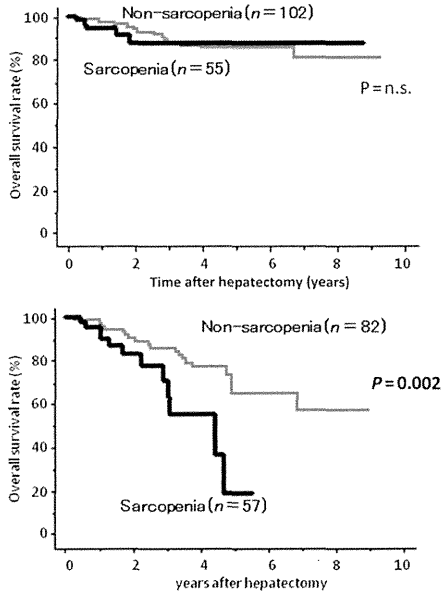


Figure 1 Overall survival curves in patients with sarcopenia or without sarcopenia in patients younger than 70 years (a) and 70 years and older (b). Overall survival rates in patients with sarcopenia indicated significantly poor prognosis in the group aged 70 years and older. n.s., Not significant.

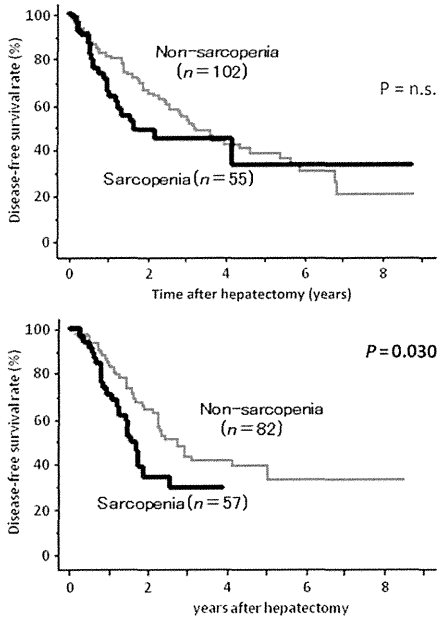


Figure 2 Disease-free survival rates in patients younger than 70 years (a) and aged 70 years and older (b) with or without sarcopenia. Disease-free survival rates in patients with sarcopenia correlated with significantly poor prognosis in the older age group. n.s., Not significant.

but the number with sarcopenia was not different between the two groups. Elderly patients had significantly lower serum albumin levels, lower level of PNI, percentage of liver cirrhosis, and histological im compared with the younger patient group. There were no significant differences regarding other host-related factors, tumor-related factors, or surgical outcome between the two groups.

Figure 1 shows OS curves in patients with or without sarcopenia. Overall survival curves are shown in patients younger than 70 years (Fig. 1a) and those 70 years of age and older (Fig.1b). Overall survival rates in patients with sarcopenia were significantly correlated with poor prognosis in patients aged ≥70 years ($P = 0.002$). Figure 2 shows DFS rates in patients with or without sarcopenia in patients younger than 70 years (Fig. 2a) and those aged ≥70 years (Fig. 2b). Disease-free survival rates in patients with sarcopenia also significantly associated with poor prognosis in the older patient group ($P = 0.030$).

**Table 2** Cox proportional hazard model of the all clinical characteristics on overall survival using univariable and multivariable analyses in patients 70 years of age and older

| | Univariable analysis | | Multivariable analysis | |
|---|---|---|---|---|
| Variables | Hazard ratio | *P*-value | Hazard ratio | *P*-value |
| Gender (male) | 0.869 (0.387, 1.955) | 0.7349 | | |
| HBs Ag(+) | 1.692 (0.401, 7.142) | 0.4738 | | |
| HCV ab(+) | 1.757 (0.815, 3.787) | 0.1503 | | |
| Diabetes mellitus | 0.951 (0.426, 2.118) | 0.9028 | | |
| Sarcopenia (+) | 3.125 (1.470, 6.622) | 0.0030 | 2.544 (1.206, 5.5865) | 0.0199 |
| Body mass index, kg/m$^2$ | 0.873 (0.780, 0.978) | 0.0192 | | |
| Albumin, g/dL | 0.651 (0.303, 1.403) | 0.2736 | | |
| Total bilirubin, mg/dL | 0.794 (0.297, 2.126) | 0.6465 | | |
| AST, IU/L | 0.985 (0.970, 1.001) | 0.0593 | | |
| Platelet count, $10^4/\mu L$ | 0.982 (0.931, 1.035) | 0.4965 | | |
| ICGR15, % | 1.013 (0.970, 1.059) | 0.5521 | | |
| CRP, mg/dL | 1.155 (0.863, 1.547) | 0.3318 | | |
| PNI | 0.950 (0.896, 1.008) | 0.0875 | | |
| Child–Pugh B | 7.751 (2.597, 23.25) | 0.0002 | 7.751(1.439, 29.41) | 0.0149 |
| Liver cirrhosis, lf + lc | 1.295 (0.653, 2.564) | 0.4591 | | |
| Tumor size, cm | 1.001 (0.888, 1.127) | 0.9911 | | |
| Multiple tumor number | 2.439 (1.157, 5.154) | 0.0191 | 2.695 (1.205, 6.024) | 0.0158 |
| Stage (III + IV) | 1.342 (0.646, 2.785) | 0.4302 | | |
| Poor differentiation (+) | 2.375 (1.191, 4.739) | 0.0140 | 3.521 (1.667, 7.463) | 0.0010 |
| mvi (+) | 1.639 (0.604, 2.450) | 0.5826 | | |
| im (+) | 1.644 (0.576, 4.695) | 0.3528 | | |
| AFP, ng/mL | 1.000 (1.000, 1.000) | 0.3092 | | |
| DCP, mAU/L | 1.000 (1.000, 1.000) | 0.0638 | | |
| Operative procedures (Anatomical) | 1.479 (0.739, 2.958) | 0.2686 | | |
| Operative time, min | 1.001 (0.998, 1.003) | 0.7028 | | |
| Estimated blood loss, g | 1.000 (1.000, 1.001) | 0.5613 | | |
| Blood transfusion (+) | 1.960 (0.843, 4.566) | 0.1177 | | |
| Postoperative complications (+) | 1.472 (0.638, 3.401) | 0.3637 | | |
| Postoperative hospital stay, days | 1.012 (0.996, 1.029) | 0.1353 | | |

Values in parentheses are 95% confidence intervals.
AFP, α-fetoprotein; AST, aspartate aminotransferase; CRP, C reactive protein; DCP, des-γ-carboxy prothrombin; HBs Ag, hepatitis B surface antigen-positive; HCV ab, hepatitis C antibody-positive; ICGR15, indocyanine green dye retention test at 15 min; im, intrahepatic metastasis; lc, liver cirrhosis; lf, liver fibrosis; mvi, microvascular invasion; PNI, prognostic nutrition index; poor differentiation, poorly differentiated hepatocellular carcinoma; Stage, TNM stage defined by the Liver Cancer Study Group of Japan.

The prognostic factors for OS and DFS in patients 70 years of age and older, according to univariate and multivariate analyses, are shown in Tables 2, 3, respectively. The significant prognostic factors for OS in the univariate analysis were presence of sarcopenia, Child–Pugh B, multiple tumor number, and poor differentiation. The significant prognostic factors for RFS in the univariate analysis were presence of sarcopenia, serum C reactive protein levels, tumor size, multiple tumor number, stage III + IV disease, presence of im, blood loss, and blood transfusion. Multivariate analysis identified four poor prognostic factors (sarcopenia, multiple tumor number, Child–Pugh B, and poor differentiation) that influenced OS, and three poor prognostic factors (sarcopenia, stage III + IV disease, and blood transfusion) that influenced DFS.

Table 4 shows the comparison of clinicopathological factors between the two groups classified by sarcopenia in patients 70 years of age and older. Patients with sarcopenia had less skeletal muscle, were more likely to be hepatitis B positive, and less likely to be hepatitis C negative. There were no significant differences regarding other parameters between the two groups in patients 70 years of age and older.

**Table 3** Cox proportional hazard model of all clinical characteristics on disease-free survival using univariable and multivariable analysis in patients with hepatocellular carcinoma aged 70 years and older

| | Univariable analysis | | Multivariable analysis | |
|---|---|---|---|---|
| Variables | Hazard ratio | *P*-value | Hazard ratio | *P*-value |
| Gender (male) | 1.733 (0.903, 3.324) | 0.0981 | | |
| HBs Ag(+) | 1.244 (0.879, 3.984) | 0.7133 | | |
| HCV ab(+) | 0.829 (0.507, 1.355) | 0.4559 | | |
| Diabetes mellitus | 0.675 (0.372, 1.222) | 0.1948 | | |
| Sarcopenia (+) | 1.766 (1.048, 2.976) | 0.0324 | 1.821 (1.037, 3.194) | 0.0366 |
| Body mass index, kg/m$^2$ | 0.958 (0.889, 1.032) | 0.2555 | | |
| Albumin, g/dL | 0.940 (0.562, 1.572) | 0.8129 | | |
| Total bilirubin, mg/dL | 1.043 (0.529, 2.055) | 0.9039 | | |
| AST, IU/L | 0.998 (0.991, 1.004) | 0.4929 | | |
| Platelet count, $10^4/\mu L$ | 0.985 (0.950, 1.020) | 0.3968 | | |
| ICGR15, % | 1.021 (0.990, 1.053) | 0.1810 | | |
| CRP, mg/dL | 1.347 (1.144, 1.587) | 0.0004 | | |
| PNI | 0.976 (0.941, 1.012) | 0.1876 | | |
| Child–Pugh B | 3.058 (1.066, 8.772) | 0.0376 | | |
| Liver cirrhosis, lf + lc | 1.075 (0.650, 1.776) | 0.7786 | | |
| Tumor size, cm | 1.087 (1.009, 1.171) | 0.0291 | | |
| Multiple tumor number | 2.890 (1.661, 5.025) | 0.002 | | |
| Stage (III + IV) | 2.439 (1.641, 3.606) | 0.0001 | 2.044(1.004, 4.167) | 0.0487 |
| Poor differentiation (+) | 1.436 (0.840, 2.457) | 0.1856 | | |
| mvi (+) | 1.486 (0.906, 2.433) | 0.1172 | | |
| im (+) | 3.184 (1.602, 6.329) | 0.0009 | | |
| AFP, ng/mL | 1.000 (1.000, 1.000) | 0.2427 | | |
| DCP, mAU/L | 1.000 (1.000, 1.000) | 0.1115 | | |
| Operative procedures (Anatomical) | 1.590 (0.972, 2.597) | 0.0647 | | |
| Operative time, min | 1.000 (0.998, 1.002) | 0.7304 | | |
| Estimated blood loss, g | 1.000 (1.000, 1.001) | 0.0495 | | |
| Blood transfusion (+) | 2.398 (1.266, 4.545) | 0.0073 | 2.941 (1.086, 8.000) | 0.0339 |
| Postoperative complications (+) | 0.988 (0.515, 1.893) | 0.9711 | | |
| Postoperative hospital stay, days | 1.001 (0.987, 1.016) | 0.8472 | | |

Values in parentheses are 95% confidence intervals.
AFP, α-fetoprotein; AST, aspartate aminotransferase; CRP, C reactive protein; DCP, des-γ-carboxy prothrombin; HBs Ag, hepatitis B surface antigen-positive; HCV ab, hepatitis C antibody-positive; ICGR15, indocyanine green dye retention test at 15 min; im, intrahepatic metastasis; lc, liver cirrhosis; lf, liver fibrosis; mvi, microvascular invasion; PNI, prognostic nutrition index; poor differentiation, poorly differentiated hepatocellular carcinoma; Stage, TNM stage defined by the Liver Cancer Study Group of Japan.

**Table 4** Comparison of clinicopathological factors between the two groups of patients with hepatocellular carcinoma (HCC) classified by sarcopenia, aged 70 years and older

| Variables | With sarcopenia ($n = 57$) | Without sarcopenia ($n = 82$) | *P*-value |
|---|---|---|---|
| Age, years | 76.5 ± 3.9 | 75.9 ± 4.0 | 0.345 |
| Male / female | 40/17 | 58/24 | 0.943 |
| HBV | 6 (10.5%) | 1 (1.2%) | 0.019 |
| HCV | 27 (47.3%) | 56 (68.3%) | 0.021 |
| Skeletal muscle mass, $cm^2/m^2$ | 61.7 ± 10.7 | 77.4 ± 9.8 | <0.001 |
| Body mass index, $kg/m^2$ | 23.3 ± 3.2 | 23.0 ± 3.5 | 0.6445 |
| Diabetes mellitus | 15 (26.3%) | 25 (30.5%) | 0.4373 |
| Albumin, g/dL | 3.8 ± 0.4 | 3.9 ± 0.5 | 0.9717 |
| Total bilirubin, mg/dL | 0.8 ± 0.4 | 0.8 ± 0.43 | 0.9345 |
| AST, IU/L | 44 ± 33 | 49 ± 35 | 0.4086 |
| Platelet count, $10^4/\mu L$ | 16.1 ± 6.7 | 16.4 ± 6.9 | 0.8190 |
| ICGR15, % | 14.5 ± 7.5 | 14.9 ± 7.5 | 0.7520 |
| CRP | 0.60 ± 1.74 | 0.28 ± 0.64 | 0.1427 |
| PNI | 45.7 ± 5.9 | 46.3 ± 6.8 | 0.6090 |
| Child–Pugh A/B | 53/4 | 78/4 | 0.7164 |
| Hepatitis grade, none / mild / severe | 10/43/4 | 11/63/8 | 0.3695 |
| Liver cirrhosis, nl + ch/lf + lc | 38/19 | 45/37 | 0.2176 |
| Tumor size, cm | 4.0 ± 2.8 | 4.0 ± 3.0 | 0.9012 |
| Solitary / multiple | 44/13 | 72/10 | 0.1095 |
| Stage, I / II / III / IV | 9/31/14/3 | 15/42/21/4 | 0.9758 |
| Differentiation, well / mod / poor | 3/41/13 | 10/52/20 | 0.829 |
| mvi (+) | 18 (31.5%) | 30 (36.5%) | 0.889 |
| im (+) | 5 (8.8%) | 7(8.5%) | 0.961 |
| AFP, ng/mL | 3890 ± 22 484 | 2231 ± 7743 | 0.539 |
| DCP, mAU/L | 1923 ± 8969 | 4910 ± 28 291 | 0.4427 |
| (Anatomical / non-anatomical) | 23/34 | 34/48 | 0.8956 |
| Operative time, min | 329 ± 107 | 344 ± 117 | 0.4649 |
| Estimated blood loss, g | 625 ± 640 | 612 ± 540 | 0.9026 |
| Blood transfusion (+) | 9(17.3%) | 14(17.0%) | 0.876 |
| Postoperative complications | 7 (12.2%) | 15 (18.3%) | 0.4791 |
| Postoperative hospital stay, days | 15 ± 11 | 18 ± 17 | 0.2330 |

Data are expressed as means ± standard deviations or number of patients (percentage) as appropriate. AFP, α-fetoprotein; AST, aspartate aminotransferase; ch, chronic hepatitis; CRP, C reactive protein; DCP, des-γ-carboxy prothrombin; HBV, hepatitis B antigen-positive; HCV, hepatitis C antibody-positive; ICGR15, indocyanine green dye retention test at 15 min; im, intrahepatic metastasis; lc, liver cirrhosis; lf, liver fibrosis; mod, moderately differentiated HCC; mvi, microvascular invasion; PNI, prognostic nutrition index; nl, normal liver; poor, poorly differentiated HCC; Stage, TNM stage defined by the Liver Cancer Study Group of Japan; well, well differentiated HCC.

Prognostic nutrition index was correlated with skeletal muscle mass (PNI = 40.019 + 0.086 × skeletal muscle mass, $r^2 = 0.030$, $P = 0.045$) (Fig. 3) in elderly patients.

## DISCUSSION

USING MULTIVARIATE ANALYSIS, this retrospective study indicated that sarcopenia is an independent prognostic factor for OS and DFS among patients 70 years of age and older with HCC. This is the first report to discuss the relationship between sarcopenia and prognosis in elderly patients with HCC after hepatectomy.

Our previous study[13] revealed the relationship between sarcopenia and prognosis, but subgroup analysis regarding aging was not investigated. With the proportion of elderly increasing rapidly worldwide, it is feared that the number of patients with sarcopenia may gradually increase in the forthcoming years, especially in cancer patients.

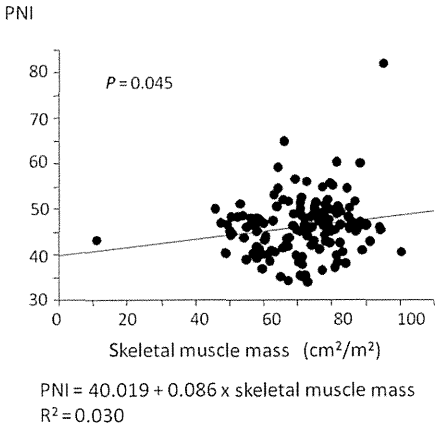


Figure 3 Prognostic nutrition index (PNI) was weakly correlated with skeletal muscle mass (PNI = 40.019 + 0.086 × skeletal muscle mass, $r^2 = 0.030$, $P = 0.045$) in elderly patients.

There are some reports that muscle mass as measured by CT is associated with the prognosis of sarcopenia.[7–13] Computed tomography is a gold standard for quantifying skeletal muscle mass, and it constitutes a good resource for objective and detailed nutritional and metabolic assessment of patients. Moreover, a CT scan is always carried out before hepatectomy, and it is a feasible method of precisely assessing sarcopenia. However, the definition of sarcopenia using CT measurement has been set using an unfounded cut-off level, and has not been accurately determined as yet, especially in Japanese people. We reported[13] survival rates in patients with sarcopenia in which cut-off values for skeletal muscle were 43.75 $cm^2/m^2$ in men and 41.10 $cm^2/m^2$ in women, according to a previous report in Germany.[8] Yoshizumi *et al.*[20] retrospectively studied healthy Japanese adults to establish formulae to calculate standard muscle area to enable an easy and accurate definition of sarcopenia. They analyzed skeletal muscle area using CT data from healthy adults and found that BSA significantly correlated with skeletal muscle area. Sarcopenia can be defined as a difference between measured and calculated data using this newly established formula. Using this criteria, sarcopenia was present in 37.8% patients with HCC compared with 40.3% in a previous report,[13] which was a similar proportion.

In this study, elderly patients had a significantly lower serum albumin levels, lower PNI levels, percentage of liver cirrhosis, and histological im compared with those aged younger than 70 years. In aging people, liver function such as serum albumin level will be gradually decreasing.[26] Inflammation-based prognostic scores such as PNI reflect the nutrition and immune status, which are useful prognostic parameters.[27,28] The PNI was correlated with skeletal muscle mass in elderly patients. Skeletal muscle in patients 70 years of age and older was significantly smaller than that of patients younger than 70 years, but the number with sarcopenia was not different between the two groups. To date, sufficient evidence exists that hepatectomy can be safely undertaken in selected elderly patients who have sufficient skeletal muscle.[14–16] The problem with this study was that it was retrospective and the population of elderly was selected.

The Child–Pugh classification was the first systematic and conventional approach used to determine the severity of cirrhosis and select patients who could tolerate hepatic resection; however, it is not always a reliable indicator of hepatic reserve, and it has a limited role in predicting postoperative outcome. To evaluate the general condition of patients before hepatectomy, no useful, objective, easy, and precise marker has been identified. The European Working Group on Sarcopenia in Older People recommends using the presence of both low muscle mass and low muscle function for the diagnosis of sarcopenia.[3] However, muscle function is difficult to evaluate, and thus, low muscle mass was investigated in this study. Among patients 70 years of age and older with HCC, there was no correlation between sarcopenia and age, sex, liver function, tumor-associated factor, or operative factor except for skeletal muscle. There is no report concerning the relationship between viral status and sarcopenia.

Among the significant prognostic factors of OS and DFS, skeletal muscle mass, tumor number, and stage can be evaluated before hepatectomy. The identification of sarcopenia patients before hepatectomy might permit early preventive strategies to maintain muscle mass in order to improve their prognosis or improve the patient selection criteria for hepatectomy.

The mechanism by which sarcopenia shortens the survival of malignant patients remains poorly understood. Skeletal muscle was recently identified as an endocrine organ.[6] It has therefore been suggested that cytokines and other peptides are produced, expressed, and released by muscle fibers, such as tumor necrosis factor-α, interleukin-6, and insulin-like growth factor 1. Low levels of skeletal muscle also indicate a systemic inflammatory response. Further study is needed to clarify the molecular mechanism concerning muscle–liver cross-talk.

This retrospective analysis revealed that sarcopenia was predictive of a worse OS and RFS after hepatectomy in

patients aged 70 years and older with HCC. As the aging population increases, this information will be useful for elderly people who need surgery.

## REFERENCES


1 WHO Interesting facts about ageing. Available at: http://www.who.int/ageing/about/facts/en/. Accessed March 15, 2016.
2 Rosenberg I. Summary comments: epidemiological and methodological problems in determining nutritional status of older persons. *Am J Clin Nutr* 1989; **50**: 1231–3.
3 Cruz-Jentoft AJ, Baeyens JP, Bauer JM *et al.* European Working Group on Sarcopenia in Older People. Sarcopenia: European consensus on definition and diagnosis: Report of the European Working Group on Sarcopenia in Older People. *Age Ageing* 2010; **39**(4): 412–23.
4 Makary MA, Segev DL, Pronovost PJ *et al.* Frailty as a predictor of surgical outcomes in older patients. *J Am Coll Surg* 2010; **210**(6): 901–8.
5 Baumgartner RN, Koehler KM, Gallagher D *et al.* Epidemiology of sarcopenia among the elderly in New Mexico. *Am J Epidemiol* 1998; **147**: 755–63.
6 Pedersen BK, Febbraio MA. Muscles, exercise and obesity: skeletal muscle as a secretory organ. *Nat Rev Endocrinol* 2012; **8**(8): 457–65.
7 Tan BH, Birdsell LA, Martin L *et al.* Sarcopenia in an overweight or obese patient is an adverse prognostic factor in pancreatic cancer. *Clin Cancer Res* 2009; **15**(22): 6973–9.
8 van Vledder MG, Levolger S, Ayez N *et al.* Body composition and outcome in patients undergoing resection of colorectal liver metastases. *Br J Surg* 2012; **99**(4): 550–7.
9 Sabel MS, Lee J, Cai S *et al.* Sarcopenia as a prognostic factor among patients with stage III melanoma. *Ann Surg Oncol* 2011; **18**(13): 3579–85.
10 Montano-Loza AJ, Meza-Junco J, Prado CM *et al.* Muscle wasting is associated with mortality in patients with cirrhosis. *Clin Gastroenterol Hepatol* 2012; **10**(2): 166–73.
11 Englesbe MJ, Patel SP, He K *et al.* Sarcopenia and mortality after liver transplantation. *J Am Coll Surg* 2010; **211**(2): 271–8.
12 Masuda T, Shirabe K, Ikegami T *et al.* Sarcopenia is a prognostic factor in living donor liver transplantation. *Liver Transpl* 2014; **20**(4): 401–7.
13 Harimoto N, Shirabe K, Yamashita YI *et al.* Sarcopenia as a predictor of prognosis in patients following hepatectomy for hepatocellular carcinoma. *Br J Surg* 2013; **100**(11): 1523–30.
14 Shirabe K, Kajiyama K, Harimoto N *et al.* Early outcome following hepatic resection in patients older than 80 years of age. *World J Surg* 2009; **33**(9): 1927–32.
15 Menon KV, Al-Mukhtar A, Aldouri A *et al.* Outcomes after major hepatectomy in elderly patients. *J Am Coll Surg* 2006; **203**(5): 677–83.
16 Aldrighetti L, Arru M, Calori G *et al.* Impact of age on the outcome of liver resections. *Am Surg* 2004; **70**(5): 453–60.
17 Taketomi A, Kitagawa D, Itoh S *et al.* Trends in morbidity and mortality after hepatic resection for hepatocellular carcinoma: an institute's experience with 625 patients. *J Am Coll Surg* 2007; **204**(4): 580–7.
18 Shirabe K, Kanematsu T, Matsumata T *et al.* Factors linked to early recurrence of small hepatocellular after hepatectomy: univariate and multivariate analyses. *Hepatology* 1991; **14**: 802–5.
19 Shimada M, Takenaka K, Fujiwara Y *et al.* Risk factors linked to postoperative morbidity in patients with hepatocellular carcinoma. *Br J Surg* 1998; **85**: 195–8.
20 Yoshizumi T, Shirabe K, Nakagawara H *et al.* Skeletal muscle area correlates with body surface area in healthy adults. *Hepatol Res* 2014; **44**(3): 313–8.
21 Liver Cancer Study Group of Japan. *General rules for the clinical and pathological study of primary liver cancer*, 2nd English edn. Tokyo: Kanehara & Co., 2003; 34–5.
22 Dindo D, Demartines N, Clavien PA. Classification of surgical complications: a new proposal with evaluation in a cohort of 6336 patients and results of a survey. *Ann Surg* 2004; **240**(2): 205–13.
23 Yamashita Y, Hamatsu T, Rikimaru T *et al.* Bile leakage after hepatic resection. *Ann Surg* 2001; **233**: 45–50.
24 Rahbari NN, Koch M, Mehabi A *et al.* Portal triad clamping versus vascular exclusion for vascular control during hepatic resection: a systematic review and meta-analysis. *J Gastrointest Surg* 2009; **13**: 558–68.
25 Shimada M, Takenaka K, Gion T *et al.* Prognosis of recurrent hepatocellular carcinoma: a 10-year surgical experience in Japan. *Gastroenterology* 1996; **111**(3): 720–6.
26 Baumgartner RN, Koehler KM, Romero L *et al.* Serum albumin is associated with skeletal muscle in elderly men and women. *Am J Clin Nutr* 1996; **64**(4): 552–8.
27 Kinoshita A, Onoda H, Imai N *et al.* Comparison of the prognostic value of inflammation-based prognostic scores in patients with hepatocellular carcinoma. *Br J Cancer* 2012; **107**(6): 988–93.
28 Pinato DJ, North BV, Sharma R. A novel, externally validated inflammation-based prognostic algorithm in hepatocellular carcinoma: the prognostic nutritional index (PNI). *Br J Cancer* 2012; **106**(8): 1439–45.

EBioMedicine 2 (2015) 1607–1612

Contents lists available at ScienceDirect

EBioMedicine

journal homepage: www.ebiomedicine.com

Research Article

# A Nationwide Survey of Hepatitis E Virus Infection and Chronic Hepatitis E in Liver Transplant Recipients in Japan

Yuki Inagaki [a,1], Yukio Oshiro [a,1], Tomohiro Tanaka [b], Tomoharu Yoshizumi [c], Hideaki Okajima [d], Kohei Ishiyama [e], Chikashi Nakanishi [f], Masaaki Hidaka [g], Hiroshi Wada [h], Taizo Hibi [i], Kosei Takagi [j], Masaki Honda [k], Kaori Kuramitsu [l], Hideaki Tanaka [m], Taiji Tohyama [n], Toshihiko Ikegami [o], Satoru Imura [p], Tsuyoshi Shimamura [q], Yoshimi Nakayama [r], Taizen Urahashi [s], Kazumasa Yamagishi [t], Hiroshi Ohnishi [u], Shigeo Nagashima [u], Masaharu Takahashi [u], Ken Shirabe [c], Norihiro Kokudo [v], Hiroaki Okamoto [u], Nobuhiro Ohkohchi [a,*]

[a] Division of Gastroenterological and Hepatobiliary Surgery, and Organ Transplantation, Department of Surgery, Faculty of Medicine, University of Tsukuba, 1-1-1 Tennodai, Tsukuba, Ibaraki 305-8575, Japan
[b] Organ Transplantation Service, The University of Tokyo Hospital, 7-3-1 Hongo, Bunkyo-ku, Tokyo 113-8655, Japan
[c] Department of Surgery and Science, Graduate School of Medical Sciences, Kyushu University, 3-1-1 Maidashi, Higashi-ku, Fukuoka 812-8582, Japan
[d] Division of Hepato-Biliary-Pancreatic and Transplant Surgery, Department of Surgery, Kyoto University Hospital, 54 Kawaharacho, Syogoin, Sakyu-ku, Kyoto 606-8507, Japan
[e] Department of Gastroenterology and Metabolism, Division of Frontier Medical Science, Programs for Biomedical Research, Graduate School of Biomedical Science, Hiroshima University, 1-2-3 Kasumi, Minami-ku, Hiroshima 734-8551, Japan
[f] Department of Transplantation, Reconstruction and Endoscopic Surgery, Tohoku University Hospital, 1-1 Seiryo-machi, Aoba-ku, Sendai, Miyagi 980-8574, Japan
[g] Department of Surgery, Nagasaki University Graduate School of Biomedical Sciences, 1-7-1 Sakamoto, Nagasaki 852-8501, Japan
[h] Department of Surgery, Graduate School of Medicine, Osaka University, 2-15 Yamadaoka, Suita, Osaka 565-0871, Japan
[i] Department of Surgery, School of Medicine, Keio University, 35 Shinano-machi, Shinjuku-ku, Tokyo 160-0016, Japan
[j] Department of Gastroenterological Surgery, Okayama University Graduate School of Medicine, Dentistry and Pharmaceutical Sciences, 2-5-1 Shikada-machi, Kita-ku, Okayama 700-8558, Japan
[k] Department of Transplantation and Pediatric Surgery, Graduate School of Medical Science, Kumamoto University, 1-1-1 Honjo, Kumamoto-shi, Kumamoto 860-8556, Japan
[l] Division of Hepato-Biliary-Pancreatic Surgery, Department of Surgery, Kobe University Graduate School of Medicine, 7-5-2 Kusunoki-cho, Chuo-ku, Kobe, Hyogo 650-0017, Japan
[m] Department of Pediatric Surgery, Faculty of Medicine, University of Tsukuba, 1-1-1 Tennodai, Tsukuba, Ibaraki 305-8575, Japan
[n] Department of HPB and Breast Surgery, Ehime University Graduate School of Medicine, Shitsukawa, To-on, Ehime 791-0295, Japan
[o] Department of Transplant Surgery, Shinshu University, School of Medicine, 3-1-1 Asahi, Matsumoto, Nagano 390-8621, Japan
[p] Department of Surgery, Institute of Biomedical Sciences, Tokushima University Graduate School, 3-18-15 Kuramoto-cho, Tokushima 770-8503, Japan
[q] Division of Organ Transplantation, Hokkaido University Hospital, Kita 14, Jonishi 5-chome, Kita-ku, Sapporo, Hokkaido 060-8648, Japan
[r] Department of Hepatobiliary Pancreatic Surgery, Juntendo University School of Medicine, 3-1-3 Hongo, Bunkyo-ku, Tokyo 113-8431, Japan
[s] Department of Transplant Surgery, Jichi Medical University School of Medicine, 3311-1 Yakushiji, Shimotsuke, Tochigi 329-0498, Japan
[t] Department of Public Health Medicine, Faculty of Medicine, University of Tsukuba, 1-1-1 Tennodai, Tsukuba, Ibaraki 305-8575, Japan
[u] Division of Virology, Department of Infection and Immunity, Jichi Medical University School of Medicine, 3311-1 Yakushiji, Shimotsuke, Tochigi 329-0498, Japan
[v] Hepato-Biliary-Pancreatic Surgery Division, Artificial Organ and Transplantation Division, Department of Surgery, Graduate School of Medicine, University of Tokyo, 7-3-1 Hongo, Bunkyo-ku, Tokyo 113-8655, Japan

ARTICLE INFO

*Article history:*
Received 14 July 2015
Received in revised form 16 September 2015
Accepted 16 September 2015
Available online 24 September 2015

*Keywords:*
Hepatitis E virus
Chronic hepatitis E
Liver transplantation
Transfusion

ABSTRACT

*Background:* Recently, chronic hepatitis E has been increasingly reported in organ transplant recipients in European countries. In Japan, the prevalence of hepatitis E virus (HEV) infection after transplantation remains unclear, so we conducted a nationwide cross-sectional study to clarify the prevalence of chronic HEV infection in Japanese liver transplant recipients.
*Methods:* A total of 1893 liver transplant recipients in 17 university hospitals in Japan were examined for the presence of immunoglobulin G (IgG), IgM and IgA classes of anti-HEV antibodies, and HEV RNA in serum.
*Findings:* The prevalence of anti-HEV IgG, IgM and IgA class antibodies was 2.9% (54/1893), 0.05% (1/1893) and 0% (0/1893), respectively. Of 1651 patients tested for HEV RNA, two patients (0.12%) were found to be positive and developed chronic infection after liver transplantation. In both cases, HEV RNA was also detected in one of the blood products transfused at the perioperative period. Analysis of the HEV genomes revealed that the HEV isolates obtained from the recipients and the transfused blood products were identical in both cases, indicating transfusion-transmitted HEV infection.

* Corresponding author.
*E-mail address:* nokochi3@md.tsukuba.ac.jp (N. Ohkohchi).
[1] These authors contributed equally to this work.

http://dx.doi.org/10.1016/j.ebiom.2015.09.030

*Interpretation:* The prevalence of HEV antibodies in liver transplant recipients was 2.9%, which is low compared with the healthy population in Japan and with organ transplant recipients in European countries; however, the present study found, for the first time, two Japanese patients with chronic HEV infection that was acquired via blood transfusion during or after liver transplantation.



## 1. Introduction

Hepatitis E is caused by infection with the hepatitis E virus (HEV), and HEV isolates that infect humans are currently categorized into four genotypes (1–4) (Okamoto, 2007). Genotypes 1 and 2 are restricted to humans and mainly waterborne transmitted in developing countries. In contrast, genotypes 3 and 4 are known to undergo zoonotic transmission by consumption of uncooked or undercooked meat or viscera of reservoir mammals and autochthonous isolates cause sporadic infections in industrialized countries (Takahashi et al., 2003; Tei et al., 2003).

Acute hepatitis E varies in severity from inapparent to fulminant. Mortality has been reported to be between 1% and 4% in the general population but up to 25% in pregnant women (Datta et al., 1987). HEV infection has traditionally been considered to be a transient and self-limiting disease requiring no specific therapy in immunocompetent individuals (Wedemeyer et al., 2012). However, HEV infection may occasionally cause severe liver dysfunction, fulminant hepatitis, and liver failure in some patients with an underlying disease (Kamar et al., 2012; Suzuki et al., 2002). Furthermore, HEV genotype 3 can lead to chronic hepatitis and liver cirrhosis in immunocompromised patients such as solid-organ transplant (SOT) recipients (Kamar et al., 2008), patients with human immunodeficiency virus infection (Dalton et al., 2009), and patients with hematologic cancers receiving chemotherapy (Ollier et al., 2009). Various studies have investigated the presence of HEV infection in SOT recipients in European and American countries but not yet in Japan. We conducted the first nationwide survey to clarify the prevalence of HEV antibodies and the presence of liver transplant recipients with chronic HEV infection in Japan.

## 2. Methods

### 2.1. Study Subjects

From all the regions of Japan, 17 high-volume centers for liver transplantation participated in this study (from north to south): Hokkaido University Hospital in Hokkaido; Tohoku University Hospital in the Tohoku area; University of Tsukuba Hospital, University of Tokyo Hospital, Keio University Hospital and Juntendo University Hospital in the Kanto area; Shinshu University Hospital in the Chubu area; Kyoto University Hospital, Osaka University Hospital and Kobe University Hospital in the Kinki area; Okayama University Hospital and Hiroshima University Hospital in the Chugoku area; Ehime University Hospital and Tokushima University Hospital in the Shikoku area; and Kyushu University Hospital, Nagasaki University Hospital and Kumamoto University Hospital in the Kyushu area. The number of liver transplantations performed in these 17 centers accounts for approximately 75% of the total performed in Japan (The Japanese Liver Transplantation Society, 2014).

Between April 1, 2013 and December 31, 2014, blood samples were collected from 1893 recipients being followed up at the above-mentioned 17 centers after liver transplantation. Anti-HEV antibodies were tested for in all 1893 samples. Within all the 1893 participants, 1651 patients who agreed to have HEV RNA testing, including all patients with detectable anti-HEV Ig (immunoglobulin) G class antibody, were also tested for the presence of HEV RNA in serum. The samples were stored at −80 °C until testing. The clinical data of the patients, including medical history, medication profiles and laboratory test results, were retrieved from medical records. This study was approved by the institutional review board at every participating hospital and performed in accordance with the Declaration of Helsinki and ethical guidelines for clinical research. All the patients gave written informed consent to participate in this study.

### 2.2. Detection of Anti-HEV Antibodies and HEV RNA

To detect anti-HEV IgA, IgM and IgG class antibodies, in-house enzyme-linked immunosorbent assay (ELISA) was performed using purified recombinant ORF2 protein as described previously (Mizuo et al., 2002). The optical density (OD) of each sample was read at 450 nm. The cut-off value used for anti-HEV IgA, IgM and IgG was 0.642, 0.440 and 0.175, respectively (Takahashi et al., 2005). The samples with OD values for anti-HEV IgA, IgM, or IgG equal to or greater than the respective cut-off value were considered to be positive for each antibody. The specificity of ELISA was validated by absorption with the same recombinant ORF2 protein that was used as the antigen probe, as described previously (Takahashi et al., 2005).

Total RNA was extracted from 100 μL of each serum or whole blood sample and subjected to nested reverse transcription-polymerase chain reaction (RT-PCR) for the detection of HEV RNA. A nested RT-PCR targeting the 137-nt ORF2/3 overlapping region was conducted for the screening of HEV RNA (Inoue et al., 2006). This method represents a high sensitivity and is able to detect 1–3 copies of HEV RNA in 100 μL serum. For the samples detected positive by the ORF2/3–137 PCR, we performed an additional nested RT-PCR targeting the 457-nt ORF2 region to confirm the presence of HEV RNA and to assess the subgenotype, as described previously (Mizuo et al., 2002). The HEV genotype/subgenotype was determined based on the phylogenetic analysis of the ORF2 sequence.

Quantitation of HEV RNA was performed by real-time detection RT-PCR as described previously (Takahashi et al., 2008).

## 3. Results

### 3.1. Characteristics of the Subjects

A total of 1893 liver transplant recipients participated in this study; their demographic characteristics and laboratory data are presented in Table 1. Median age was 57 years old and median time since liver transplantation to serum sampling was 81 months. At the time of blood sampling, the median values of aspartate aminotransferase (AST), alanine aminotransferase (ALT), total bilirubin (T-Bil) and gamma-glutamyl transferase (γ-GT) were exclusively within normal limits. "Liver injury episode after transplantation" was defined as the presence of elevated liver enzymes acquiring the management with re-hospitalization, and 61.3% of the recipients were included.

### 3.2. Prevalence of Anti-HEV Antibodies and HEV RNA

All of the 1893 serum samples were subjected to ELISA for the detection of anti-HEV antibodies (Table 2). Fifty-four patients (2.9%) were found to be positive for anti-HEV IgG class antibody. The age- and sex-specific prevalence of IgG class antibody in the recipients is shown in Fig. 1. The prevalence was slightly higher among the males (3.3%) than among the females (2.4%), although not statistically significant, and generally increased with age. Only one patient with detectable IgG class antibody was also positive for IgM class antibody (0.05%),

**Table 1**
Characteristics of liver transplant recipients.a

| | |
|---|---|
| Total number of recipients [n] | 1893 |
| Age [years; median (total range)] | 57 (0–83) |
| Sex [n (%); male/female] | 970 (51.2)/923 (48.8) |
| Time from transplantation [months; median (total range)] | 81 (0–297) |
| *Laboratory data at sampling* | |
| WBC [/μL; median (total range)] | 5565 (1070–97,000) |
| Lymphocyte [/μL; median (total range)] | 1576 (157–24,225) |
| AST [IU/L; median (total range)] | 24 (1–484) |
| ALT [IU/L; median (total range)] | 19 (3–619) |
| T-Bil [mg/dL; median (total range)] | 0.8 (0.1–40.0) |
| γ-GT [IU/L; median (total range)] | 36 (0–3118) |
| Immunosuppression [n (%)] | |
| Tacrolimus/cyclosporin | 1359 (71.8)/327 (17.3) |
| Mycophenolic acid | 685 (36.2) |
| Corticosteroids | 681 (36.0) |
| Re-hospitalization due to liver injury episode after transplantation[a] [n (%)] | 1161 (61.3) |

Note: WBC, white blood cell; AST, aspartate aminotransferase; ALT, alanine aminotransferase; T-Bil, total bilirubin; γ-GT, gamma-glutamyl transferase.
[a] Liver injury episode after transplantation was defined as the presence of elevated liver enzymes acquiring the management with re-hospitalization.

while none had detectable IgA class antibody. In this patient, who was positive for IgG and IgM antibodies, HEV RNA was also detectable as noted below.

Two of the 54 patients with anti-HEV IgG tested positive for HEV RNA, while none of the remaining 1597 patients without detectable IgG class antibody who agreed to have the HEV RNA testing were positive for HEV RNA. Overall, HEV RNA was found to be positive at the prevalence rate of 0.12% (2/1651) (Table 2). The detailed clinical information and laboratory data at the time of diagnosis in these two HEV RNA-positive patients are shown in Table 3. Case 1 patient was a 60-year-old female living in the Kanto area who received liver transplantation for primary sclerosing cholangitis, while Case 2 patient was a 41-year-old male living in the Kyushu area who received liver transplantation for non-alcoholic steatohepatitis complicated with hepatocellular carcinoma. In these two patients, the duration from liver transplantation to blood sampling was lower than the 25 percentile (36 months), and the peripheral blood lymphocyte count was lower than the 25 percentile (1039 /μL). Whereas 71.8% and 35.9% of the patients negative for HEV RNA had been taking tacrolimus and corticosteroids respectively, both two positive patients had been taking tacrolimus and corticosteroids for immunosuppression. The HEV isolates were typed as genotype 3 in both patients (Table 3). The more detailed clinical courses of these two patients will be described elsewhere.

### 3.3. Elucidation of Possible Infectious Source and Route

To clarify whether these two HEV-viremic patients contracted HEV infection during or after liver transplantation and to investigate the possible infectious route of HEV in these patients, we retrospectively tested anti-HEV antibodies and HEV RNA in stored serum samples from each pair of patient and liver donor (Table 4).

In Case 1 patient, anti-HEV IgG class antibody was weakly positive; representing past HEV infection, while HEV RNA was not detected in the pre-transplant serum. Anti-HEV IgG became high-titer positive (OD value: >3.000) on the 255th postoperative day (POD) accompanied by high-titer HEV RNA ($8.1 \times 10^5$ copies/mL), and HEV RNA was persistently positive on the 360th POD. In Case 2 patient, anti-HEV IgG and IgM antibodies and HEV RNA were negative in the pre-transplant serum. On the 81st POD, the positive conversion of IgG and IgM antibodies was detected accompanied by high-titer HEV RNA ($1.3 \times 10^6$ copies/mL). HEV RNA was persistently positive on the 249th POD. These results suggested that both patients acquired their HEV infection during or after liver transplantation and developed chronic infection of HEV. In addition, retrospective and prospective investigation of their laboratory data and virological analysis revealed that these recipients had presented mild liver injury and HEV viremia for at least more than 6 months. Therefore, these two patients were finally diagnosed as having chronic hepatitis E.

**Table 2**
*Prevalence of HEV antibodies and HEV RNA in liver transplant recipients.a*

| | Positive patient [n] | Percent [%] |
|---|---|---|
| Anti-HEV IgG | 54/1893 | 2.9 |
| Anti-HEV IgM | 1/1893 | 0.05 |
| Anti-HEV IgA | 0/1893 | 0 |
| HEV RNA | 2/1651[a] | 0.12 |

Note: Ig, immunoglobulin.
[a] The number of patients whose informed consent for testing HEV RNA was available.

In both cases, HEV antibodies and HEV RNA were undetectable in the liver donors, excluding the possibility of de novo HEV infection from the transplanted liver. The two HEV-viremic patients had no history of eating raw or undercooked meat or shellfish after liver transplantation. During the perioperative period of liver transplantation, a total of 17 units of blood products (concentrated red blood cells, fresh frozen plasma or platelets) were transfused in Case 1 patient, and 26 units of blood products (concentrated red blood cells, fresh frozen plasma or platelets) transfused in Case 2 patient. Pilots of all the blood products transfused during the perioperative period had been stored in the Japanese Red Cross Society, and were also tested for the presence of HEV RNA. HEV RNA was detectable in one unit of the fresh frozen plasma transfused to Case 1 patient (the viral titer was not available) and one unit of the platelet preparation transfused to Case 2 patient (the viral titer was $1.8 \times 10^4$ copies/mL). Complete nucleotide sequence identity was obtained in the 412-nt sequence of ORF2 of each HEV isolate. As a result, in both cases, the HEV isolates detected from the recipient and the blood product were considered to be same, and the transfused blood products were determined to be the infectious source.

## 4. Discussion

HEV infection had not been considered responsible for chronic hepatitis until Kamar et al. reported the first case series of chronic hepatitis E in SOT recipients in 2008 (Kamar et al., 2008). Subsequently, chronic infections of HEV in transplant recipients have been described in several studies (Haagsma et al., 2009; Legrand-Abravanel et al., 2010). According to the latest review article in 2014, up to 50–60% of acute HEV infections can progress to chronic phase in SOT recipients and HEV infection can take rapid courses leading to liver cirrhosis in patients receiving immunosuppressants (Behrendt et al., 2014). Despite the high prevalence of HEV in the SOT recipients in European countries, chronic hepatitis E in Asian countries has been rarely reported (Behrendt et al., 2014).

By 2013, over 7000 liver transplants had been performed in Japan (The Japanese Liver Transplantation Society, 2014). The number of national notifications of acute hepatitis E has been increasing since anti-HEV IgA antibody measurement started to be covered by insurance in 2011 (The National Institute of Infectious Diseases. Infectious Diseases Weekly Report (IDWR), 2003–2013), and the isolation of autochthonous HEV as a causative agent of acute hepatitis has increased. However, no nationwide survey of HEV infection in liver transplant recipients had been performed. So the present study is the first nationwide survey to investigate the prevalence of HEV infection in liver transplant recipients in Japan. This large multicenter severance clarified that the presence of HEV infection in liver transplant recipients is not frequent in Japan compared with in Western countries as described below. However, two cases of transfusion-transmitted hepatitis E were detected; therefore, recipients have low but certain risk of HEV infection by blood products.

Though more than 60% of the recipients had some kind of episode of liver injury, the values of liver enzymes, T-Bil and γ-GT were exclusively within normal limits at the time of sampling. These episodes of liver injury were most commonly due to the biliary complication or the